Oligosaccharides Display Both Rigidity and High Flexibility in Water as Determined by ^{13}C NMR Relaxation and $^{1}H,^{1}H$ NOE Spectroscopy: Evidence of *anti*-ϕ and *anti*-ψ Torsions in the Same Glycosidic Linkage

Christer Höög, Clas Landersjö, and Göran Widmalm*[a]

Abstract: The trisaccharide β-D-Glc*p*-$(1\rightarrow2)$-β-D-Glc*p*-$(1\rightarrow3)$-α-D-Glc*p*-OMe has been investigated by molecular dynamics (MD) simulations and NMR experiments in water. ^{13}C spin-lattice (T_1) and spin–spin (T_2) relaxation times, together with $^{1}H,^{13}C$ NOE data were measured at two magnetic field strengths (9.4 and 14.1 T) in a 277 K D_2O solution. Relaxation data interpreted by means of the model-free formalism revealed a rigid ($S^2\sim0.9$) oligosaccharide tumbling in solution. $^{1}H,^{1}H$ Cross-relaxation rates were determined at 600 MHz by 1D DPFGSE NOESY and T-ROESY experiments, which provided high quality data and subsequently proton–proton distances within the trisaccharide. The presence of *anti* conformers at both torsions of a glycosidic linkage is demonstrated for the first time. MD simulations were carried out to facilitate analysis of the NOE data. In total, 15 simulations—starting from five different conformational states—were performed, with production runs of up to 10 ns, resulting in 83 ns of oligosaccharide dynamics in water. *anti* Conformers were populated to different degrees in the simulations, especially at the ϕ_2 torsion angle. By combining the results from the NOE experiments and the MD simulations, the *anti* conformers at the $(1\rightarrow2)$-linkage were quantified as 7% *anti*-ϕ_2 and 2% *anti*-ψ_2, revealing a highly flexible trisaccharide in which large conformational changes occur. From the MD simulations, interresidue hydrogen bonding, from HO2″ to O2 or O3, was significantly populated ($\sim$40%) in both of the *anti* conformational states. The contentious issue over rigidity versus flexibility in oligosaccharides has thus been thoroughly examined, showing that the dynamics should be taken into account for a relevant description of the molecular system.

Keywords: carbohydrates · molecular dynamics · NMR spectroscopy · oligosaccharides

Introduction

In nature, carbohydrates are commonly found interacting with different biomolecules, proteins in particular, but also with other carbohydrate molecules. The carbohydrate portion, being important in biochemical regulation and control, is often conjugated to lipids or proteins. The structures of oligosaccharides and polysaccharides are closely related to their functions and the ability to modify the saccharides by means of various functional groups or by combinations of different stereoisomers, as well as positional isomers, makes the combinatorial coding capacity of saccharides unsurpassed.[1] Cellular recognition can be mediated by proteins, known as lectins, which specifically recognize different carbohydrate structures.[2] The influence of structure on oligosaccharide conformation, both in solution and when bound to a protein receptor, is therefore a major topic of interest.[3, 4] X-ray crystallographic studies are often not feasible, nor will they necessarily give the same result as in solution. NMR spectroscopy, then, is the method of choice for solution studies, combined to varying degrees with molecular modeling.[5–7]

The original work on oligosaccharide conformation by Lemieux and co-workers[8–11] laid the foundations for the understanding of their three dimensional structures. A simplified molecular mechanics force field, based on the *exo*-anomeric effect and modeling the sugar residues as "hard spheres", was also implemented. This is referred to as the HSEA approach and can be used for rapid determination of relevant low energy conformations of oligosaccharides. Full molecular mechanics force fields for carbohydrates have subsequently been developed for investigation of oligosaccharide conformations.[12, 13] These force fields are continuously being refined to obtain greater accuracy in reproduction of structural and energetic trends.[14] Recent modeling studies on oligosaccharide conformation have focused on the influence and structure of the surrounding solvent.[15, 16]

[a] Prof. Dr. G. Widmalm, Dr. C. Höög, Dr. C. Landersjö
Department of Organic Chemistry
Arrhenius Laboratory Stockholm University
106 91 Stockholm (Sweden)
Fax: (+46) 815-4908
E-mail: gw@organ.su.se

  0947-6539/01/0714-3069 $ 17.50+.50/0

A great deal of work has been dedicated not only to the pyranose ring flexibility,[17] but also to the flexibility at the glycosidic linkage.[18] Molecular modeling has been used to try to assess the flexibility at the glycosidic torsion angles ϕ and ψ.[19] As a first approximation of oligosaccharide conformation, a *syn* relationship with torsion angles in the vicinity of 0° is a good estimate. More recently, on the basis of NMR spectroscopic findings, the existence of *anti*-ψ[20] and *anti*-ϕ[21] conformers (~180°) has been demonstrated. These studies both employed dimethyl sulfoxide as solvent to facilitate the detection of *anti* conformers. An *anti*-ψ conformer was shown to be present in an oligosaccharide bound to an antibody, albeit not at a glycosidic linkage of the primary recognition unit.[22] As well as this, a glycosidic linkage constrained to an *anti*-ψ conformer has recently been described.[23]

Experimental NMR data, such as ^{1}H,^{1}H nuclear Overhauser effects (NOEs), have been used to infer flexibility at the glycosidic linkage, since the fit to a conformationally averaged structure was better than to a single conformation.[24] More explicit information has been obtained from ^{13}C magnetic field-dependent relaxation measurements on oligosaccharides and interpreted by the model-free formalism of Lipari and Szabo.[25] The generalized order parameter was significantly lower than unity, which is indicative of internal motion,[26, 27] if the molecule tumbles isotropically.[28] Other ways to investigate oligosaccharide conformation by NMR spectroscopy are by measurement of long-range *trans*-glycosidic coupling constants, either ^3J(C,H)[29] or ^3J(C,C),[30] related to the torsion angles through the Karplus equations. More recently, oligosaccharide conformation has been addressed by analysis of residual dipolar couplings in dilute liquid crystalline media.[31–33]

The use of a solvent other than water to identify *anti* conformers of oligosaccharides in solution is warranted as a means to obtain knowledge of the carbohydrate conformation. However, it poses the problem that the conformation may be induced or stabilized in a manner not possible in water. In the study identifying an *anti*-ϕ conformation[21] in the trisaccharide β-D-Glc*p*-(1→2)-β-D-Glc*p*-(1→3)-α-D-Glc*p*-OMe we used Langevin dynamics[34] (LD) simulations in order to obtain a trajectory of sufficient duration (50 ns). In LD, the solvent is modeled by stochastic and dissipative forces and unless any specific stabilization—such as intramolecular hydrogen bonding—occurs, this technique may be a good approximation. However, for xylobiose the vacuum adiabatic Ramachandran energy map and the free energy map in aqueous solution were shown to differ significantly, with a bridging water molecule hydrogen bonding to a hydroxyl group on each sugar residue.[15]

To remedy the possible deficiencies of the above approach, we have investigated the trisaccharide β-D-Glc*p*-(1→2)-β-D-Glc*p*-(1→3)-α-D-Glc*p*-OMe (**1**) by molecular dynamics (MD) simulations in water and with high quality 1D NOE and transverse rotating-frame Overhauser effect (T-ROE) NMR experiments to ascertain whether the *anti*-ϕ conformation is present at the (1→2)-linkage in water solution. Moreover, the simulations and experimental data facilitate investigation of the presence of an *anti*-ψ conformation at the same glycosidic linkage. Furthermore, ^{13}C relaxation measurements in water, ^{1}H,^{1}H NOE and T-ROE experiments and the MD simulations make it possible for us to address the issue of rigidity versus flexibility in oligosaccharides. We will show that the apparent inconsistency of the two is a function of the analysis and the timescale of the processes and that a unified representation of oligosaccharide conformation and dynamics can be obtained.

Theory

Relaxation of proton-bearing ^{13}C nuclei is usually dominated by dipole–dipole interactions with neighboring protons. Assuming that chemical shift anisotropy and cross-correlation effects are negligible, the relaxation parameters for carbons with directly bonded protons can be calculated from the spectral density functions, $J(\omega)$:[35]

$$T_1^{-1} = \frac{1}{4}(D_{CH})^2[J(\omega_H - \omega_C) + 3J(\omega_C) + 6J(\omega_H+\omega_C)] \quad (1)$$

$$T_2^{-1} = \frac{1}{8}(D_{CH})^2[4J(0) + J(\omega_H - \omega_C) + 3J(\omega_C) + 6J(\omega_H) + 6J(\omega_H+\omega_C)] \quad (2)$$

$$\eta = \left(\frac{\gamma_H}{\gamma_C}\right)\frac{6J(\omega_H + \omega_C) - J(\omega_H - \omega_C)}{J(\omega_H - \omega_C) + 3J(\omega_C) + 6J(\omega_H + \omega_C)} \quad (3)$$

The dipolar coupling constant, $D_{CH} = (\mu_0/4\pi)\gamma_C\gamma_H\hbar r_{CH}^{-3}$—where μ_0 is the permittivity of free space, r_{CH} is the proton–carbon internuclear distance, γ_H and γ_C are the magnetogyric ratios for proton and carbon, respectively, and $\hbar$ is Planck's constant divided by 2π. A value of 111.7 pm is used for r_{CH}.[36] For carbons with two directly bonded protons, the relaxation rates T_1^{-1} and T_2^{-1} can be obtained by multiplying the calculated rates by a factor of two.

The model-free approach developed by Lipari and Szabo can be used to interpret the relaxation data in terms of motional parameters.[25] On the assumption that overall tumbling is isotropic and that its correlation time, τ_M, is much larger than the correlation time for internal reorientation, τ_e, the reduced spectral density function becomes:

$$J(\omega) = \frac{2}{5}\left(\frac{S^2\tau_M}{1+\omega^2\tau_M^2} + \frac{(1-S^2)\tau}{1+\omega^2\tau^2}\right) \quad (4)$$

where $\tau^{-1} = \tau_M^{-1} + \tau_e^{-1}$. The spatial restriction of the CH vector local motion is described by the generalized order parameter, S^2. If the first term in Equation (4) is much larger than the second, the equation can be truncated to obtain:

$$J(\omega) = \frac{2}{5}\left(\frac{S^2\tau_M}{1+\omega^2\tau_M^2}\right) \quad (5)$$

For molecules in solution, the proton relaxation is dominated by the dipolar interactions between protons that are close in space. The strength of these interactions is dependent on the dipolar coupling constant of the protons (D_{HH}) and consequently the distance (r) between them. The cross-

0947-6539/01/0714-3070 $ 17.50+.50/0 *Chem. Eur. J.* **2001**, *7*, No. 14

relaxation rate, σ, for NOE and ROE can be expressed as combinations of spectral density functions taken at zero frequency, the proton Larmor frequency and at twice the proton Larmor frequency. The nuclear Overhauser effect (NOE)[37] is measured in the laboratory frame and the cross-relaxation rate is given by:

$$\sigma_{NOE} = \frac{1}{4}(D_{HH})^2[6J(2\omega) - J(0)] \quad (6)$$

The rotating-frame Overhauser effect (ROE)[38] has its cross-relaxation rate given by:

$$\sigma_{ROE} = \frac{1}{4}(D_{HH})^2[2J(0) + 3J(\omega)] \quad (7)$$

Using the spin lock conditions devised by Hwang and Shaka,[39] the multi-pulse or transverse ROE (T-ROE) cross relaxation rate, $\sigma_{T\text{-}ROE}$, can be calculated as the mean of σ_{NOE} and σ_{ROE} and is described by:

$$\sigma_{T\text{-}ROE} = \frac{1}{8}(D_{HH})^2[6J(2\omega) + 3J(\omega) + J(0)] \quad (8)$$

Although the value of $\sigma_{T\text{-}ROE}$ will be smaller than that of σ_{ROE}, the T-ROESY pulse sequence has the advantage that it efficiently suppresses signals arising from TOCSY transfer,[40, 41] a problem encountered with the ordinary ROESY pulse sequence.

If a reference proton–proton pair of known separation in the molecule can be obtained, the isolated spin-pair approximation (ISPA),[42, 43] makes it possible to extract unknown distances between protons i and j by comparing cross-relaxation rates according to:

$$r_{ij} = r_{ref}\,(\sigma_{ref}/\sigma_{ij})^{1/6} \quad (9)$$

If no reference distance is available, or the dynamics for the reference proton pair differ from the dynamics of the proton pair for which the distance is sought, the interproton distances may be calculated using the combinations of spectral density functions, in the form, for example, of the model-free approach by Lipari and Szabo.

Results and Discussion

The conformational flexibility and dynamics of the trisaccharide β-D-Glc*p*-(1→2)-β-D-Glc*p*-(1→3)-α-D-Glc*p*-OMe in water solution have been investigated here by MD simulations and different NMR spectroscopy experiments. A schematic drawing of **1** is shown in Figure 1. ^{13}C NMR relaxation experiments in oligosaccharides have been used as a tool to demonstrate the presence of internal motion.[44] Measurement of longitudinal (T_1) and transverse (T_2) relaxation times as well as ^1H,^{13}C NOE at 277 K and two magnetic field strengths showed that the trisaccharide was outside the extreme narrowing region in which $T_1 \neq T_2$ (Table 1). The central residue shows shorter relaxation times and a lower heteronuclear NOE. The relaxation data were used to calculate the model-free parameters S^2 and τ_M, which are the generalized order parameter—a measure of spatial restriction of motion—and the correlation time for overall reorientation, respectively.

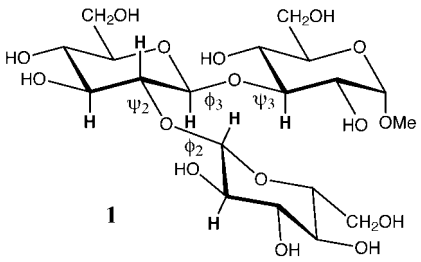

Figure 1. Schematic representation of the trisaccharide β-D-Glc*p*-(1→2)-β-D-Glc*p*-(1→3)-α-D-Glc*p*-OMe (**1**) in a *syn* conformation of the torsion angles at the glycosidic linkages. Protons for which *trans*-glycosidic Overhauser effects were measured are denoted in bold.

Table 1. Averaged relaxation data for ring carbons of each residue in trisaccharide **1** at 277 K and results from two-parameter, least-squares fits of individual sugar residues.

B_0 [T]		β-D-Glc*p*-(1→	→2)-β-D-Glc*p*-(1→	→3)-α-D-Glc*p*-OMe
9.4	T_1	279[a]	238	264
	T_2	231	217	230
	$1+\eta$	2.12	1.98	2.04
14.1	T_1	344	302	328
	$1+\eta$	1.77	1.62	1.70
	τ_M [ns]	0.42 ± 0.02	0.48 ± 0.03	0.45 ± 0.02
	S^2	0.87 ± 0.03	0.93 ± 0.03	0.88 ± 0.02
	Δy[b]	3.8	3.7	3.0

[a] T_1 and T_2 values are given in ms. [b] Standard deviation of the dependent variable (%).

The truncated form of the Lipari/Szabo equation, that is Equation (5), was successfully used, whereas when Equation (4) was tried the errors in the fitting process became large. This is consistent with our previous studies; that is, when the generalized order parameter is high, the short correlation time cannot be obtained with confidence.[45] These results show a highly rigid molecule, with $S^2 \approx 0.9$ for the three residues and a $\tau_M \approx 0.45$ ns. The flexibility of the three hydroxymethyl groups was restricted, with essentially the same $S^2 = 0.8$ (data not shown). Thus, the ^{13}C relaxation data shows the trisaccharide to be a highly rigid entity with only some librational motion. This is illustrated in Figure 2 as an

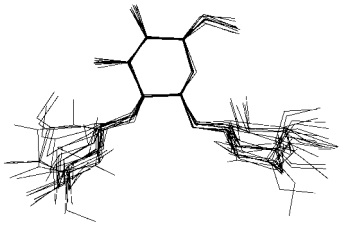

Figure 2. Overlay plot from MD simulation based on the central residue of **1**, showing eight random structures of *syn* conformation.

overlay plot generated from the MD simulations (see below) for the trisaccharide in the *syn* conformational state. The extraction of motional properties in **1** also served a second purpose, to facilitate the determination of proton–proton distances from ^{1}H,^{1}H cross-relaxation rates as described below.

The MD simulations were started from five different conformations: one all *syn* and four *anti*, in which one of the torsions was changed. These are denoted *syn* (simulation I), *anti*-ϕ_2 (II), *anti*-ψ_2 (III), *anti*-ϕ_3 (IV), and *anti*-ψ_3 (V). From the *syn* conformation, nine simulations were started with different initial velocities. Additional runs were also performed for simulations II and III. The combination of different starting conformers and initial velocities was used to facilitate varied sampling of the conformational space. In total, 15 simulations were carried out, with production runs of 1.5 to 10.0 ns, resulting in 83 ns of oligosaccharide simulation in water, summarized in Table 2.

Table 2. Glycosidic torsion angle averages and root-mean-square (rms) fluctuations from the simulations of **1**.

Simulation	Time [ns]	$\langle\phi_2\rangle$ [°]	$\langle\psi_2\rangle$ [°]	$\langle\phi_3\rangle$ [°]	$\langle\psi_3\rangle$ [°]
I a	4.0	19 (29)	67 (40)	100 (52)	15 (22)
I b	7.5	103 (50)	10 (29)	61 (25)	6 (26)
I c	10.0	102 (57)	17 (28)	72 (39)	9 (27)
I d	4.5	86 (50)	165 (172)	57 (15)	1 (24)
I e	7.0	77 (49)	−3 (39)	57 (14)	5 (25)
I f	6.5	126 (51)	2 (48)	55 (14)	0 (25)
I g	10.0	94 (59)	96 (147)	65 (36)	32 (83)
I h	3.5	53 (36)	−125 (87)	53 (13)	6 (22)
I i	4.5	107 (56)	13 (28)	57 (14)	1 (25)
II a	2.5	94 (61)	−45 (85)	53 (15)	1 (25)
II b	3.5	123 (48)	24 (23)	59 (17)	4 (28)
III a	5.5	84 (55)	4 (41)	67 (34)	5 (26)
III b	4.0	89 (52)	−27 (78)	54 (14)	3 (26)
IV	8.5	154 (25)	16 (14)	53 (14)	−5 (23)
V	1.5	46 (28)	0 (20)	41 (16)	155 (39)

On the timescale of these simulations—that is, several ns—the torsions of the (1→2)-linkage have not converged whereas those relating to the (1→3)-linkage have. The conformational space sampled is demonstrated by scatter plots from simulation I e (Figure 3). We note that the flexibility during the 7 ns simulation is significantly greater at the (1→2)-linkage than at the (1→3)-linkage. Trajectory analysis of simulation I g (Figure 4) reveals that an *anti*-ϕ_2 conformation is visited several times during the 10 ns timespan. An *anti*-ϕ_3 conformation is also populated in this trajectory, but to a lesser degree. *anti*-ψ Torsions are visited once at each glycosidic linkage. Analysis of all simulations shows that, of the folded conformations, the *anti*-ϕ_2 conformation is the most pronounced and that the other *anti* conformations may be populated transiently. Simulation V showed $\langle\psi_3\rangle = 155°$. However, it was started in the *anti*-ψ_3 conformation, which lasted for ≈1.4 ns when a transition to a *syn* conformation took place. After that, the simulation was not continued any further. Like the previous LD simulations, the current MD simulations in water also particularly support

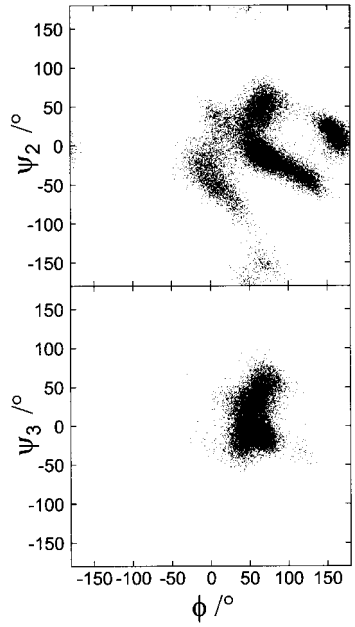

Figure 3. Scatter plots from MD simulation I e, showing the conformational regions sampled by the glycosidic linkages in the trisaccharide (top: (1→2)-linkage; bottom: (1→3)-linkage).

an *anti*-ϕ_2 conformation. To investigate the presence of the *anti* conformers revealed above, we performed additional NMR experiments.

^{1}H,^{1}H Cross-relaxation rates, σ_{NOE} and $\sigma_{T\text{-}ROE}$, were obtained in water for trisaccharide **1**, using 1D DPFGSE NOESY and T-ROESY experiments. Selective excitations of anomeric proton signals were performed (Figure 5) and a series of different mixing times were used in order to obtain NOE and T-ROE build-up curves (Figure 6). From the initial slope of the build-up curves, it was possible to derive the cross-relaxation rates (Table 3). The motional properties of **1** determined above (Table 1) were used together with the appropriate ^{1}H,^{1}H cross-relaxation rates and Equations (5) and (6) or Equations (5) and (8) to calculate proton–proton distances.[46] These results are also given in Table 3. The consistency of proton–proton distances obtained from NOE and T-ROE experiments is excellent, the distance between H1″ and H2′, for example, is 2.30 Å as calculated from both experiments. The *trans*-glycosidic distances differ somewhat, with H1′–H3 being shorter than H1″–H2′. For comparison and a further measure of the quality of the data, a reference distance—namely, H1′–H3′ (well resolved for integration)—was chosen and determined as 2.50 Å by simulation. The direct determinations described above (2.48 and 2.55 Å) are in very good agreement with this distance. Using Equation (9) (ISPA), proton–proton distances were calculated (Table 3). In particular, the agreement of the former analysis with that when a reference distance is assumed is very good.

We have previously analyzed oligosaccharide conformation by comparing experimental NOE build-up curves to those obtained by MD simulation by a full relaxation matrix approach.[47] In that analysis, an effective reorientational correlation time was required as input. Another approach would be to calculate spectral density functions from MD

0947-6539/01/0714-3072 $ 17.50+.50/0 *Chem. Eur. J.* **2001**, *7*, No. 14

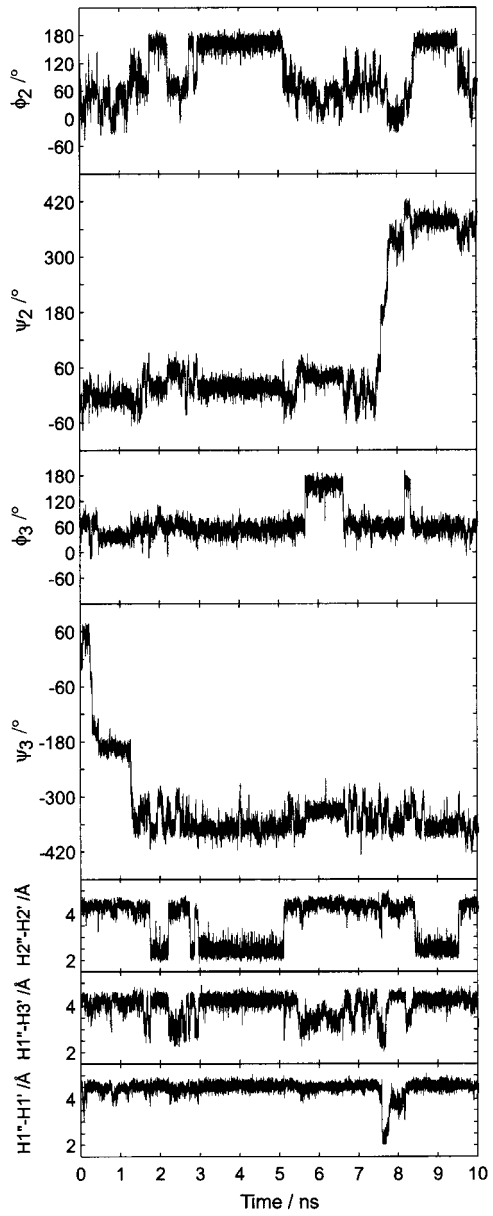

Figure 4. MD trajectories of torsion angles and selected proton–proton distances in **1** from simulation I g.

Table 3. Cross-relaxation rates, σ_{NOE} and $\sigma_{T\text{-}ROE}$, for the trisaccharide in water at 277 K. Interproton distances r calculated using τ_M and S^2 from the ^{13}C relaxation measurements (model-free approach) and the isolated spin-pair approximation (ISPA).

Proton pair		Model-free approach				ISPA	
Excited	Detected	σ_{NOE} [s^{-1}]	$\sigma_{T\text{-}ROE}$ [s^{-1}]	r_{NOE} [Å]	$r_{T\text{-}ROE}$ [Å]	r_{NOE} [Å]	$r_{T\text{-}ROE}$ [Å]
H1″	H2′	– 0.078	0.169	2.30	2.30	2.42	2.28
H1′	H3	– 0.124	0.275	2.06	2.12	2.24	2.11
H2″	H2′		0.016		3.41		3.38
H1″	H3′	– 0.009	0.012	3.30	3.58	3.48	3.55
H1′	H1″		0.010		3.69		3.66
H1′	H3′	– 0.064	0.098	2.48	2.55	2.50[a]	2.50[a]

[a] Reference distance from MD simulation.

simulation and subsequently for NMR parameters to be compared with those obtained from measurements.[48] However, the issue in this investigation is that of oligosaccharide

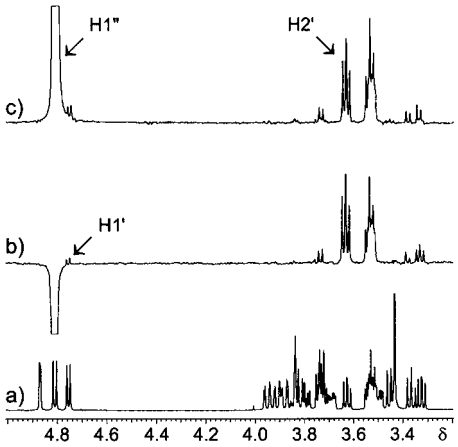

Figure 5. ^1H NMR spectrum of **1** in D_2O at 277 K a). Selective excitation of H1″, showing the 1D $^1H,^1H$ T-ROESY b) and NOESY c) spectra with a mixing time of 600 ms. Pertinent protons are annotated.

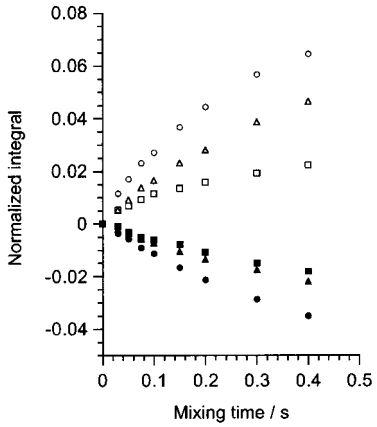

Figure 6. $^1H,^1H$ Cross-relaxation build-up curves obtained by selective excitation of anomeric protons of β-linked residues in **1**. T-ROESY data denoted by open symbols and NOESY data by filled symbols. The Overhauser effects were observed for H1′–H3 (circles), H1″–H2′ (triangles), and H1′–H3′ (squares).

rigidity versus flexibility. We therefore chose to compare proton–proton distances averaged as $\langle r^{-6}\rangle^{-1/6}$[49] in different conformational states from the MD simulation. Thus, the librational motion in each conformational state is then taken into account in the analysis.

The proton–proton distances in three conformational states and two full MD simulations, averaged as $\langle r^{-6}\rangle^{-1/6}$, are reported in Table 4. In the *syn* state (Figure 7, part a) H1′–H3 < H1″–H2′. The distances are somewhat longer than those determined experimentally, most probably due to larger librational motions in the *syn* state, revealing that further force field development is needed for an even better agreement. From the two 10 ns simulations I c and I g, distances are quite well converged. The distance between H2″ and H2′ (Figure 4 and Table 4) is sensitive to the *anti*-ϕ_2 conformation (Figure 7, part b).

The H2″ resonance (most upfield in the ^1H NMR spectrum) was therefore selectively excited and a T-ROE build-up curve generated (Figure 8). The resulting experimentally determined H2″–H2′ distance was 3.41 Å (Table 3), significantly shorter than in the all *syn* conformational state (4.12 Å), but

Table 4. Interproton distances r [Å] in the trisaccharide, extracted from the simulations and averaged according to $r = \langle r^{-6} \rangle^{-1/6}$.

Proton pair	*syn*[a]	*anti*-ϕ_2[b]	*anti*-ψ_2[c]	Ic	Ig
H1″–H2′	2.47	3.42	3.61	2.76	2.62
H1′–H3	2.40	2.31	2.32	2.45	2.44
H2″–H2′	4.12	2.34	4.48	2.64	2.70
H1″–H3′	3.57	4.04	2.53	3.59	3.63
H1″–H1′	4.03	4.51	2.21	4.39	4.00

[a] Simulation IIIa: 3.5–5.5 ns. [b] Simulation IV: 0–8.5 ns. [c] Simulation Ih: 0.3–2.5 ns.

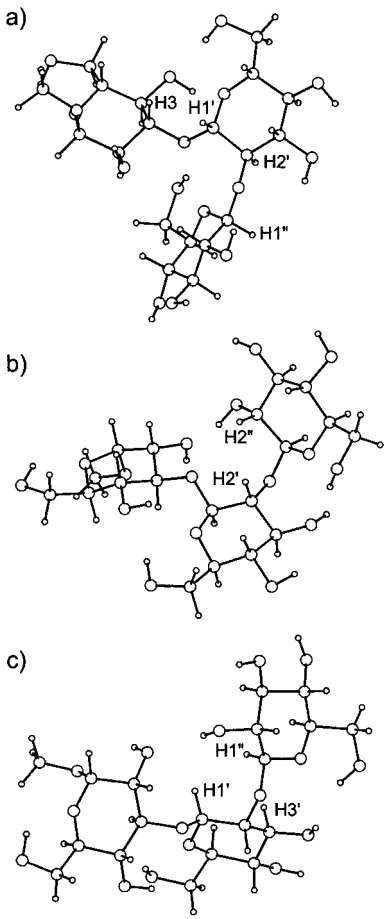

Figure 7. Snapshots from MD simulations of **1**, showing for the torsion angles at the $(1\rightarrow2)$-linkage: a *syn* conformer a), an *anti*-ϕ_2 conformer b), and an *anti*-ψ_2 conformer c). Protons essential for the characterization of each conformational state are annotated.

longer than in the *anti*-ϕ_2 conformational state (2.34 Å). The simulation and experimental data may be used in a two-state analysis:

$$(1-x)\langle r_{syn}^{-6}\rangle + (x)\,\langle r_{anti}^{-6}\rangle = r_{\exp}^{-6} \qquad (10)$$

where x is the fraction that populates the *anti* state. This reveals the presence of ~7% *anti*-ϕ_2 conformation. The MD simulations, however, overestimate the population of the *anti*-ϕ_2 conformation at this torsion angle but do correctly predict its presence. Using ab initio molecular orbital calculations in the conformational analysis of equatorial 2-methoxytetrahydropyran, Tvaroska and Carver showed that the relative

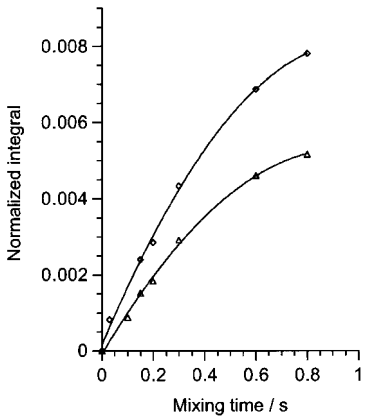

Figure 8. ^{1}H,^{1}H Cross-relaxation build-up curves from T-ROESY experiment of **1** obtained by selective excitation of H2″ (diamonds) and H1′ (triangles), showing NOE to H2′ and H1″, respectively.

energy difference between a *syn* conformer in the "*exo*-anomeric effect conformation" and an *anti*-ϕ conformation is ~3 kcal mol^{-1}.[50] They also compared the relative energies as calculated by different molecular mechanics methods and found for the CHARMM force field that the *syn* conformer, as anticipated, was more stable than the *anti*-ϕ conformer, although the energetic difference was lower (~1 kcal mol^{-1}). It is therefore not surprising that the force field in use here overestimates the *anti*-ϕ_2 conformation. However, the fine tuning of the potentials is a delicate matter. We have observed excellent agreement between simulation and experiment using this CHARMM force field,[51] as well as differences when other recent force fields (GLYCAM and OPLS) were employed.[16] Our results show that the *anti*-ϕ_2 conformation of **1** previously shown to exist in dimethyl sulfoxide[21] is also present in water solution.

In the NOE and T-ROE spectra, an Overhauser effect between H1″ to H1′ was observed (Figure 5); this should be the product of an *anti*-ψ_2 conformation (Figure 7, part c), seen transiently in the MD simulations. Such an *anti* conformation should also show an NOE from H1″ to H3′, which should be measurable by T-ROE as well as by NOE build-up curves. For H1″–H3′, a distance of 3.30–3.58 Å was determined (Table 3). However, this is only marginally shorter than in the all *syn* conformation. Moreover, it is not exclusively sensitive to an *anti*-ψ_2 conformation (Figure 4), since $\psi_2 \approx 40^\circ$ also produces a distance of ≈3.2 Å. Instead, the cross-relaxation rate for the H1′–H1″ pair (Figure 8), which is sensitive to this state (Figure 4), was obtained, giving a distance of 3.69 Å. In comparison, the *anti*-ψ_2 conformation from the MD simulation showed a distance of 2.21 Å. The *syn* conformation averaged 4.03 Å for the H1′–H1″ pair. By the same token as for the *anti*-ϕ_2 conformation [Eq. (10)], the *anti*-ψ_2 conformation could be quantified as ~2%. Thus, the presence of both an *anti*-ϕ_2 conformation and of an *anti*-ψ_2 conformation could be both shown and *quantified* in water solution for the $(1\rightarrow2)$-linkage of **1**, revealing a highly flexible oligosaccharide (cf. Figure 7). Normalized populations of the three conformational states for this linkage are: *syn* 91%, *anti*-7% and *anti*-ψ_2 2%. For the $(1\rightarrow3)$-linkage, the above analysis was not possible, due to severe spectral overlap in the

0947-6539/01/0714-3074 $ 17.50+.50/0 *Chem. Eur. J.* **2001**, *7*, No. 14

^{1}H NMR spectrum. However, the combined results from these MD simulations, the shorter H1′–H3 distance from NMR experiments and the previously determined *trans*-glycosidic ^3J(C,H) values[21] all indicate that the contribution from *anti* conformers at this linkage is small, and in particular that *anti*-ϕ_3 is less populated than *anti*-ϕ_2.

Solvent interactions can be investigated by use of an atomic radial distribution function (RDF). This is given by $g_{nm}(r)$, where the first index *n* refers to a solute atom and the second index *m* refers to a solvent atom.[52] These were analyzed for **1** in water solution. We focused on the difference between the *syn* conformation and the *anti*-ϕ_2 and *anti*-ψ_2 conformations. The RDF $g_{HO}(r)$ for solute-hydrogen to solvent-oxygen was particularly informative. In the *anti*-ϕ_2 conformation, $g_{HO}(r)$ around O2″ showed a significantly reduced probability (Figure 9, part a). For O2, this was not as marked and hydrogen

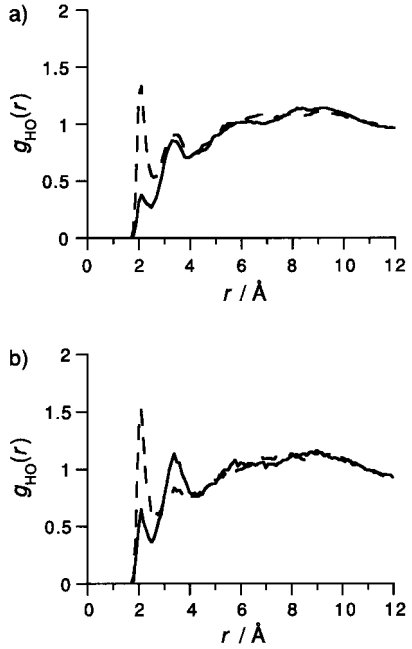

Figure 9. Radial distribution functions of **1** from MD simulation. a) *anti*-ϕ_2 conformation with $g_{HO}(r)$ around O2″ (solid line) and O2 (dashed line); b) *anti*-ψ_2 conformation with $g_{HO}(r)$ around O2″ (solid line) and O2 (dashed line).

bonding of HO2 to solvent water does take place to a large extent. A striking similarity is seen for the same $g_{HO}(r)$ in the *anti*-ψ_2 conformation (Figure 9, part b). Interresidue intramolecular hydrogen bonding in **1** was then monitored in the simulations. Specifically, HO2″ makes intramolecular hydrogen bonds to O2 (*anti*-ϕ_2) or to O2 and O3 (*anti*-ψ_2) ~40% of the time when in an *anti* conformational state (Table 5). Other hydrogen bonds such as O3′–HO6″ and O5″–HO3′ were only present in the *anti* conformers of the (1→2)-linkage. In contrast, an O4–HO6′ hydrogen bond between the (1→3)-linked residues was present in the three conformational states described above.

The issue of whether oligosaccharides should be regarded as rigid or flexible has been hotly debated during the last decade, especially as a result of the introduction of molecular dynamics simulation techniques in the field of carbohydrate

Table 5. Population of selected hydrogen bonds (%) in different conformational states of **1** from MD simulations.

Atom pair	*syn*	*anti*-ϕ_2	*anti*-ψ_2
O2–HO2″	–	40	30
O3–HO2″	–	1	14
O3′–HO6″	–	34	41
O5″–HO3′	–	9	9
O4–HO6′	48	33	48

chemistry.[19] The topic had already been addressed earlier, when disparate views existed.[53, 54] Subsequently, a number of reports from different laboratories investigating the flexibility of oligosaccharides have been published. Usually, NMR spectroscopy has been used to obtain experimental data for comparison to simulation results,[55–67] but optical rotation data[68, 69] have also been employed. This study shows that it is more appropriate to discuss the degree of flexibility of an oligosaccharide and reveals the necessity of defining the timescale being considered. What looks like a discrepancy in describing oligosaccharide **1** as both rigid and highly flexible is readily explained by taking the appropriate timescales into account. Furthermore, the quantification of the populations of different conformational states as described here affords possibilities for addressing force field development in future studies, since the molecular system has been shown to exhibit complex although not intractable behavior.

Conclusion

This study has addressed the controversy over rigidity or flexibility in oligosaccharides. We have shown by ^{13}C NMR relaxation measurements that oligosaccharides can display a quite rigid and distinct conformation over a shorter timescale: $< \tau_M$ in this case. At the same time, a high degree of flexibility of the oligosaccharide over a longer timescale—$> \tau_M$—is evident. The significant flexibility of the trisaccharide was shown to exist at its (1→2)-linkage and quantification of the *anti*-ϕ_2 and *anti*-ψ_2 conformations revealed populations of 7 and 2%, respectively. Thus, there is no inconsistency in describing oligosaccharides as being rigid or highly flexible. Rather, it is a question of dynamics. The results should therefore broaden our view of how oligosaccharides may interact in biological systems and highlights the importance of investigation of flexibility and dynamics in carbohydrate–protein interactions.

Experimental Section

General: The synthesis of the trisaccharide β-D-Glc*p*-(1→2)-β-D-Glc*p*-(1→3)-α-D-Glc*p*-OMe (**1**) has been described previously,[70] together with ^{1}H and ^{13}C NMR assignments of most resonances in D_2O. Atoms in the terminal glucosyl residue are denoted by a double prime, in the middle residue they are labeled by a prime, and in the O-methyl residue the atoms are unprimed. The torsion angles at a glycosidic linkage are denoted by ϕ_X = H1–C1–OX–CX and ψ_X = C1–OX–CX–HX, where X is the linkage atom.

NMR spectroscopy: The trisaccharide was treated with CHELEX 100 in order to remove any paramagnetic ions. The sample was freeze-dried and dissolved in 0.7 mL D_2O to give a total concentration of 50 mM, transferred to a 5 mm NMR tube, and flame-sealed under vacuum after degassing by three freeze–pump–thaw cycles. All NMR experiments were performed at 277 K, permitting measurements outside the extreme narrowing region. The assignments of the C6 signals were accomplished with the aid of a gHSQC-TOCSY experiment,[71] with a mixing time of 20 ms.

^{13}C T_1 and ^1H,^{13}C NOE experiments were performed at two magnetic field strengths, 9.4 and 14.1 T, using Varian Inova spectrometers. ^{13}C T_2 experiments were performed at the lower magnetic field strength. All ^{13}C resonances were well resolved at the higher field strength, while a slight overlap was found at 9.4 T. The relaxation data for the ring carbons were averaged over each residue, using the concept of dynamic equivalence,[72] while the methylene carbons were treated separately. The spectral window covered ~60 ppm and the number of data points was 16k. All experiments were carried out 2–3 times, independently of each other. Standard pulsed proton broad-band decoupling techniques were used, with the decoupling power attenuated in order to avoid sample heating. A deuterium lock was used for the field/frequency stabilization.

^{13}C T_1 measurements were performed by inversion-recovery experiments, using three-parameter non-linear fits of line intensities. Ten different relaxation delay times (10 ms to ~2 T_1) were used, and the pre-scan delay was >5 T_1. ^{13}C T_2 values were measured using a modification of the CPMG pulse sequence, with a proton π pulse of 26 μs, placed at even echoes in order to minimize cross-correlation effects.[73, 74] The carbon π pulse was 13 μs. Ten different relaxation delays were used, the CPMG delay was set to 0.25 ms, and the pre-scan delay was >10 T_1. Heteronuclear ^1H,^{13}C NOEs were measured with the dynamic NOE technique.[75] The experiments were performed with one short (1 ms) and one long (2.0 s) irradiation period, and a pre-scan delay of >10 T_1. The NOEs ($1+\eta$) were calculated by taking the ratio of the intensity at the long irradiation period to that of the short one. The errors of the averaged relaxation parameters are estimated to be <1% in T_1 and $1+\eta$ and ~5% in T_2.

The magnetic field-dependent T_1^{-1}, T_2^{-1}, and $1+\eta$ values for each residue were least-squares fitted simultaneously, using the program GENLSS[76] running on an SGI workstation, resulting in the model-free parameters S^2 and τ_M. Sums of squares of relative (rather than absolute) errors were minimized, allowing the measured parameters (T_1^{-1}, T_2^{-1}, and $1+\eta$) to be treated in a balanced way.

Proton–proton cross-relaxation rates (σ_{NOE} and $\sigma_{T\text{-}ROE}$) were measured at 600 MHz using one-dimensional DPFGSE NOESY[77, 78] and DPFGSE T-ROESY[79] experiments, respectively. Selective excitations at the anomeric protons and H2″ were enabled using a 20 Hz broad i-Snob-2 shaped pulse[80] of 85 ms duration. The gradient durations in the initial DPFGSE part were 1 ms and the strength 0.7 and 2.2 G cm^{-1}, respectively. In the following NOESY part of the pulse sequence, four gradients of 1 ms duration were performed in pairs with strengths 1.5 and 1.1 G cm^{-1}, respectively, with a 2 ms hyperbolic secant inversion pulse[81] inserted between the gradients in each pair. All other pulses were hard and of short duration, <8 μs for a 90° pulse. For the T-ROE experiment, the DPFGSE part was followed by a T-ROESY spin lock with $\gamma B_1/2\pi = 3.0$ kHz.

Spectra were recorded using a width of 1250 Hz and 8k complex data points. For each mixing time, 384 transients were used and the total relaxation delay between the transients was 13.3 s, which corresponds to >5 T_1. Ten different ^1H,^1H cross-relaxation delays (mixing times) between 30 and 800 ms were used. Prior to Fourier transformation, the FIDs were zero-filled to 32k datapoints and multiplied with a 2 Hz exponential line-broadening factor. Spectra were phased, drift corrected, and baseline corrected using a first-order correction, and integrated using the same integration limits at all mixing times.

Integrated auto-peaks were fitted to an exponentially decaying function, and normalized integrals of cross-relaxation peaks were obtained by division of the measured integrals by the extrapolated auto-peak value at zero mixing time. The regression coefficient in the fits was $R > 0.997$ for all autopeaks. Cross-relaxation build-up curves were obtained from the normalized integrals at different mixing times and the rates were calculated by fitting to a second-order polynomial. The least-square fits, expressed using the regression coefficient, showed $R > 0.991$ in all cases. Any contribution from "three-spin" effects on NOE build-up curves was negligible as determined by simulation using a multi-spin relaxation matrix analysis.[47]

Computer simulations: The molecular mechanics program CHARMM[82] (parallel version, C25b2) was used for all simulations with the force field PARM22 (Molecular Simulations Inc., San Diego, CA (USA)), which is similar to the carbohydrate force field developed by Ha et al.[83] Initial conditions for simulation of **1** were produced by placing the trisaccharide in a previously equilibrated cubic water box of length 29.972 Å containing 900 TIP3 water molecules, and removing those waters that were closer than 2.5 Å to any solute atom. This procedure resulted in a system with the trisaccharide and 855 ± 2 water molecules, which was energy minimized using steepest descent, 200 steps, followed by adopted basis Newton–Raphson until the root-mean-square gradient was less than 0.01 kcal mol^{-1} Å^{-1}. Velocities were initialized at 100 K, followed by heating at 5 K increments over 8 ps to 300 K, at which the systems were equilibrated for 200 ps. Constant temperature simulations were then performed using Berendsen's weak-coupling algorithm.[84] Minimum image boundary conditions were used with a heuristic non-bond frequency update and force shift cutoff[85] acting to 12 Å, using a dielectric constant of unity. SHAKE,[86] with a tolerance gradient of 10^{-4}, was used to restrain hydrogen-heavy atom bond stretch; the time step was accordingly set to 2 fs. Data were saved every 0.2 ps for analysis. Five different starting conformations were used: namely I ($\phi_2 = 60°$, $\psi_2 = 0°$, $\phi_3 = 60°$, $\psi_3 = 0°$), II ($\phi_2 = 180°$, $\psi_2 = 0°$, $\phi_3 = 60°$, $\psi_3 = 0°$), III ($\phi_2 = 60°$, $\psi_2 = 180°$, $\phi_3 = 60°$, $\psi_3 = 0°$), IV ($\phi_2 = 60°$, $\psi_2 = 0°$, $\phi_3 = 180°$, $\psi_3 = 0°$), and V ($\phi_2 = 60°$, $\psi_2 = 0°$, $\phi_3 = 60°$, $\psi_3 = 180°$). Several simulations were carried out with different initial velocities. The geometric criteria for hydrogen bonding were set to an oxygen-hydrogen distance <2.5 Å and a donor-hydrogen acceptor angle $\Theta > 135°$. Simulations were performed on an IBM SP2 computer at the Center for Parallel Computers, KTH, Stockholm, using 16 nodes resulting in a CPU time of approximately 20 h per 1 ns.

Acknowledgements

This work was supported by a grant from the Swedish Natural Science Research Council. We thank the Center for Parallel Computers, KTH, Stockholm, for putting computer facilities at our disposal and the Swedish NMR Centre, Göteborg, for providing access to the 600 MHz NMR spectrometer.

[1] H.-J. Gabius, *Pharm. Rev.* **1998**, *15*, 23–30.
[2] H. Lis, N. Sharon, *Chem. Rev.* **1998**, *98*, 637–674.
[3] E. E. Simanek, G. J. McGarvey, J. A. Jablonowski, C.-H. Wong, *Chem. Rev.* **1998**, *98*, 833–862.
[4] A. Poveda, J. Jiménez-Barbero, *Chem. Soc. Rev.* **1998**, *27*, 133–143.
[5] L. Poppe, G. S. Brown, J. S. Philo, P. V. Nikrad, B. H. Shah, *J. Am. Chem. Soc.* **1997**, *119*, 1727–1736.
[6] M. Hricovíni, M. Guerrini, A. Bisio, *Eur. J. Biochem.* **1999**, *261*, 789–801.
[7] R. Harris, G. R. Kiddle, R. A. Field, M. J. Milton, B. Ernst, J. L. Magnani, S. W. Homans, *J. Am. Chem. Soc.* **1999**, *121*, 2546–2551.
[8] R. U. Lemieux, S. Koto, *Tetrahedron* **1974**, *30*, 1933–1944.
[9] R. U. Lemieux, K. Bock, S. Koto, L. T. J. Delbaere, V. S. Rao, *Can. J. Chem.* **1980**, *58*, 631–653.
[10] H. Thøgersen, R. U. Lemieux, K. Bock, B. Meyer, *Can. J. Chem.* **1982**, *60*, 44–57.
[11] R. U. Lemieux, K. Bock, *Arch. Biochem. Biophys.* **1983**, *221*, 125–134.
[12] S. Pérez, A. Imberty, S. B. Engelsen, J. Gruza, K. Mazeau, J. Jiménez-Barbero, A. Poveda, J. F. Espinosa, B. P. van Eyck, G. Johnson, A. D. French, M. L. C. E. Kouwijzer, P. D. J. Grootenuis, A. Bernardi, L. Raimondi, H. Senderowitz, V. Durier, G. Vergoten, K. Rasmussen, *Carbohydr. Res.* **1998**, *314*, 141–155.
[13] R. J. Woods, *Rev. Comput. Chem.* **1996**, *9*, 129–165.
[14] M.-J. Hwang, X. Ni, M. Waldman, C. S. Ewig, A. T. Hagler, *Biopolymers* **1998**, *45*, 435–468.
[15] K. J. Naidoo, J. W. Brady, *J. Am. Chem. Soc.* **1999**, *121*, 2244–2252.
[16] A. Vishnyakov, G. Widmalm, J. Kowalewski, A. Laaksonen, *J. Am. Chem. Soc.* **1999**, *121*, 5403–5412.

  0947-6539/01/0714-3076 $ 17.50+.50/0

[17] S. Ernst, G. Venkataraman, V. Sasisekharan, R. Langer, C. L. Cooney, R. Sasisekharan, *J. Am. Chem. Soc.* **1998**, *120*, 2099–2107.
[18] B. J. Hardy, *J. Mol. Struct. (Theochem)* **1997**, *395–396*, 187–200.
[19] *Computer Modeling of Carbohydrate Molecules*, ACS Symp. Ser. 430 (Eds.: A. D. French, J. W. Brady), Washington, DC, **1990**.
[20] J. Dabrowski, T. Kozár, H. Grosskurth, N. E. Nifant'ev, *J. Am. Chem. Soc.* **1995**, *117*, 5534–5539.
[21] C. Landersjö, R. Stenutz, G. Widmalm, *J. Am. Chem. Soc.* **1997**, *119*, 8695–8698.
[22] M. J. Milton, D. R. Bundle, *J. Am. Chem. Soc.* **1998**, *120*, 10547–10548.
[23] A. Geyer, M. Müller, R. R. Schmidt, *J. Am. Chem. Soc.* **1999**, *121*, 6312–6313.
[24] A. Helander, L. Kenne, S. Oscarson, T. Peters, J.-R. Brisson, *Carbohydr. Res.* **1992**, 230, 299–318.
[25] G. Lipari, A. Szabo, *J. Am. Chem. Soc.* **1982**, *104*, 4546–4559; G. Lipari, A. Szabo, *J. Am. Chem. Soc.* **1982**, *104*, 4559–4570.
[26] L. Mäler, G. Widmalm, J. Kowalewski, *J. Biomol. NMR* **1996**, *7*, 1–7.
[27] A. Poveda, J. L. Asensio, M. Martín-Pastor, J. Jiménez-Barbero, *J. Biomol. NMR* **1997**, *10*, 29–43.
[28] T. Rundlöf, R. M. Venable, R. W. Pastor, J. Kowalewski, G. Widmalm, *J. Am. Chem. Soc.* **1999**, *121*, 11847–11854.
[29] T. Rundlöf, A. Kjellberg, C. Damberg, T. Nishida, G. Widmalm, *Magn. Reson. Chem.* **1998**, *36*, 839–847.
[30] B. Bose, S. Zhao, R. Stenutz, F. Cloran, P. B. Bondo, G. Bondo, B. Hertz, I. Carmichael, S. Serianni, *J. Am. Chem. Soc.* **1998**, *120*, 11158–11173.
[31] T. Rundlöf, C. Landersjö, K. Lycknert, A. Maliniak, G. Widmalm, *Magn. Reson. Chem.* **1998**, *36*, 773–776.
[32] G. R. Kiddle, S. W. Homans, *FEBS Lett.* **1998**, *436*, 128–130.
[33] P. J. Bolon, J. H. Prestegard, *J. Am. Chem. Soc.* **1998**, *120*, 9366–9367.
[34] R. W. Pastor in *The molecular dynamics of liquid crystals* (Eds.: G. R. Luckhurst, C. A. Veracini), Kluwer Academic Publishers, Dordrecht, **1994**, pp. 85–138.
[35] D. Doddrell, V. Glushko, A. Allerhand, *J. Chem. Phys.* **1972**, *56*, 3683–3689.
[36] M. Ottiger, A. Bax, *J. Am. Chem. Soc.* **1998**, *120*, 12334–12341.
[37] A. W. Overhauser, *Phys. Rev.* **1955**, *92*, 411–415.
[38] A. A. Bothner-By, R. L. Stephens, J.-M. Lee, C. D. Warren, R. W. Jeanloz, *J. Am. Chem. Soc.* **1984**, *106*, 811–813.
[39] T.-L. Hwang, A. J. Shaka, *J. Am. Chem. Soc.* **1992**, *114*, 3157–3159.
[40] T.-L. Hwang, M. Kadkhodaei, A. Mohebbi, A. J. Shaka, *Magn. Reson. Chem.* **1992**, *30*, S24–S34.
[41] T.-L. Hwang, A. J. Shaka, *J. Magn. Reson. B* **1993**, *102*, 155–165.
[42] J. W. Keepers, T. L. James, *J. Magn. Reson.* **1984**, *57*, 404–426.
[43] P. D. Thomas, V. J. Basus, T. L. James, *Proc. Natl. Acad. Sci. USA* **1991**, *88*, 1237–1241.
[44] J. Kowalewski, L. Mäler, G. Widmalm, *J. Mol. Liq.* **1998**, *78*, 255–261.
[45] A. Kjellberg, T. Rundlöf, J. Kowalewski, G. Widmalm, *J. Phys. Chem. B* **1998**, *102*, 1013–1020.
[46] L. Mäler, G. Widmalm, J. Kowalewski, *J. Phys. Chem.* **1996**, *100*, 17103–17110.
[47] B. J. Hardy, W. Egan, G. Widmalm, *Int. J. Biol. Macromol.* **1995**, *17*, 149–160.
[48] R. Brüschweiler, D. A. Case, *Prog. NMR Spectrosc.* **1994**, *26*, 27–58.
[49] D. Neuhaus, M. P. Williamson, *The nuclear Overhauser effect in structural and conformational analysis*, VCH Publishers, New York, **1989**.
[50] I. Tvaroska, J. P. Carver, *J. Phys. Chem.* **1994**, *98*, 9477–9485.
[51] C. Höög, G. Widmalm, *J. Phys. Chem. A* **2000**, *104*, 9443–9447.
[52] D. Chandler, *Introduction to Modern Statistical Mechanics*, Oxford University Press, Oxford, **1987**.
[53] C. A. Bush, Z.-Y. Yan, B. N. N. Rao, *J. Am. Chem. Soc.* **1986**, *108*, 6168–6173.
[54] R. U. Lemieux, R. Cromer, U. Spohr, *Can. J. Chem.* **1988**, *66*, 3083–3098.
[55] S. W. Homans, *Biochemistry* **1990**, *29*, 9110–9118.
[56] C. Hervé du Penhoat, A. Imberty, N. Roques, V. Michon, J. Mentech, G. Descotes, S. Pérez, *J. Am. Chem. Soc.* **1991**, *113*, 3720–3727.
[57] M. Hricovíni, R. N. Shah, J. P. Carver, *Biochemistry* **1992**, *31*, 10018–10023.
[58] T. Peters, B. Meyer, R. Stuike-Prill, R. Somorjai, J.-R. Brisson, *Carbohydr. Res.* **1993**, *238*, 49–73.
[59] K. Bock, J. Ø. Duus, S. Refn, *Carbohydr. Res.* **1994**, *253*, 51–67.
[60] G. Widmalm, R. M. Venable, *Biopolymers* **1994**, *34*, 1079–1088.
[61] J. P. M. Lommerse, L. M. J. Kroon-Batenburg, J. Kroon, J. P. Kamerling, J. F. G. Vliegenthart, *J. Biomol. NMR* **1995**, *5*, 79–94.
[62] J. L. Asensio, J. Jiménez-Barbero, *Biopolymers* **1995**, *35*, 55–73.
[63] B. J. Hardy, A. Gutierrez, K. Lesiak, E. Seidl, G. Widmalm, *J. Phys. Chem.* **1996**, *100*, 9187–9192.
[64] A. J. Petrescu, T. D. Butters, G. Reinkensmeier, S. Petrescu, F. M. Platt, R. A. Dwek, M. R. Wormald, *EMBO J.* **1997**, *16*, 4302–4310.
[65] T. Kozár, N. E. Nifant'ev, H. Grosskurth, U. Dabrowski, J. Dabrowski, *Biopolymers* **1998**, *46*, 417–432.
[66] W.-G. Wu, L. Pasternack, D.-H. Huang, K. M. Koeller, C.-C. Lin, O. Seitz, C.-H. Wong, *J. Am. Chem. Soc.* **1999**, *121*, 2409–2417.
[67] A. M. Dixon, G. Widmalm, T. E. Bull, *J. Magn. Reson.* **2000**, *147*, 266–272.
[68] B. J. Hardy, S. Bystricky, P. Kovac, G. Widmalm, *Biopolymers* **1997**, *41*, 83–96.
[69] E. P. Stroyan, E. S. Stephens, *Carbohydr. Res.* **2000**, *327*, 447–453.
[70] A. Adeyeye, P.-E. Jansson, L. Kenne, G. Widmalm, *J. Chem. Soc. Perkin Trans. 2* **1991**, 963–973.
[71] T. de Beer, C. W. E. M. van Zuylen, K. Hård, R. Boelens, R. Kaptein, J. P. Kamerling, J. F. G. Vliegenthart, *FEBS Lett.* **1994**, *348*, 1–6.
[72] J. Kowalewski, G. Widmalm, *J. Phys. Chem.* **1994**, *98*, 28–34.
[73] L. E. Kay, L. K. Nicholson, F. Delaglio, A. Bax, D. A. Torchia, *J. Magn. Reson.* **1992**, *97*, 359–375.
[74] A. G. Palmer, N. J. Skelton, W. J. Chazin, P. E. Wright, M. Rance, *Molec. Phys.* **1992**, *75*, 699–711.
[75] J. Kowalewski, A. Ericsson, R. Vestin, *J. Magn. Reson.* **1978**, *31*, 165–169.
[76] D. F. DeTar, Genlss in *Computer Programs for Chemistry*, *Vol. 4*, Academic Press, New York, **1972**, pp. 71–124.
[77] K. Stott, J. Stonehouse, J. Keeler, T.-L. Hwang, A. J. Shaka, *J. Am. Chem. Soc.* **1995**, *117*, 4199–4200.
[78] K. Stott, J. Keeler, Q. N. Van, A. J. Shaka, *J. Magn. Reson.* **1997**, *125*, 302–324.
[79] A. Kjellberg, G. Widmalm, *Biopolymers* **1999**, *50*, 391–399.
[80] É. Kupce, J. Boyd, I. D. Campbell, *J. Magn. Reson. B* **1995**, *106*, 300–303.
[81] J. Baum, R. Tycko, A. Pines, *Phys. Rev. A* **1985**, *32*, 3435–3447.
[82] B. R. Brooks, R. E. Bruccoleri, B. D. Olafson, D. J. States, S. Swaminathan, M. Karplus, *J. Comput. Chem.* **1983**, *4*, 187–217.
[83] S. N. Ha, A. Giammona, M. Field, J. W. Brady, *Carbohydr. Res.* **1988**, *180*, 207–221.
[84] H. J. C. Berendsen, J. P. M. Postma, W. F. van Gunsteren, A. DiNola, J. R. Haak, *J. Chem. Phys.* **1984**, *81*, 3684–3690.
[85] P. J. Steinbach, B. R. Brooks, *J. Comput. Chem.* **1994**, *15*, 667–683.
[86] W. F. van Gunsteren, H. J. C. Berendsen, *Molec. Phys.* **1977**, *34*, 1311–1327.

Received: December 20, 2000 [F2956]